

# An Any-Resolution Distributed Pressure Localization Scheme Using a Capacitive Soft Sensor Skin

Harshal A. Sonar<sup>1</sup>, Michelle C. Yuen<sup>1,2,3</sup>, Rebecca Kramer-Bottiglio<sup>2</sup> and Jamie Paik<sup>\*1</sup>

**Abstract**—We present a method to determine the location of an applied pressure on a large area, monolithic silicone-based capacitive sensor. In contrast to pressure sensor arrays composed of  $n \times n$  discrete sensors, we utilize a single sensor body with a single instrumentation interface to detect  $n$  pixels. We interrogate the capacitive sensor at different frequencies, thus modulating the effective length of the sensor. These interrogation frequencies are governed by the sensor’s total capacitance, resistance, and desired spatial resolution of the sensor. We developed an analytical model to calculate the frequency response at different length segments of the sensor and used the results to determine the interrogation frequencies for experimental studies. We performed experimental tests on a  $1 \times n$  sensor strip and an  $n \times n$  sensor sheet and showed that we could attain greater than 90% accuracy in predicting the location of the applied pressure using a model generated by a multi-class kernel support vector machine. This approach towards distributed localization of point pressures greatly reduces the hardware complexity in comparison to discrete sensor arrays and increases the physical robustness of the system.

## I. INTRODUCTION

Robotic systems that interact with their surroundings need to detect and localize the contact with an object. Pressure sensor arrays are a well-developed technology with multiple commercially available devices (TakkTiles, Sensitronics, Tekscan, Sensing Tex, BodiTrak, SureTouch). However, the majority of these commercial devices incorporate materials that are stiffer or more strain-limited than those commonly demanded by softer interfaces, hindering their integration.

Researchers have developed various approaches to “soften” pressure sensing for soft robotics, human-computer interactive system, and wearable applications. Two common approaches for measuring pressure are by measuring the resistance of a deformable, soft or fluid conductor or by measuring the capacitance of a deformable capacitor. Some resistive sensing approaches include the use of conductive polymer composites [1]–[3] or embedding liquid-metal microchannels in silicone elastomer [4]–[7]. Capacitive sensing approaches use a variety of materials for both the conductive electrodes and the dielectric layer. Electrode materials can be broadly classified into metal thin film [8]–[11], liquid metal [12], [13], conductive silicone composite [14]–[17], conductive fabrics [18]–[20], hydrogels [21], carbon nanotubes [22], and carbon grease [23], [24]. The dielectric layers have been

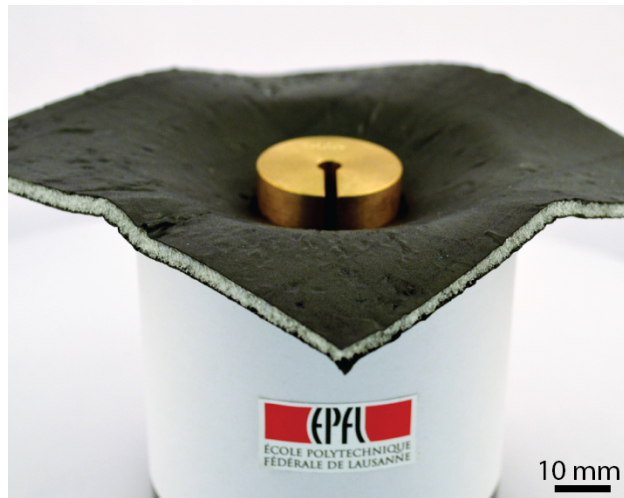


Fig. 1. The soft monolithic silicone-based capacitive sensor skin deforming into a mug. The sensor skin measures  $120 \times 120 \times 4$  mm<sup>3</sup> with 70 pF of overall capacitance.

composed of silicone foam [8], [9], [18], native silicone [11]–[15], [17], [21], [22], polyurethane [10], and acrylic foam tape [23], [24].

Though the transduction means to convert pressure to a signal may differ, the majority of these devices utilize a single sensor to make a single measurement of pressure. In order to distribute sensing capability over larger areas, researchers have patterned multiple pixels individually [5], [8], [19], [25] over the sensing region at the desired spatial resolution. However, as the number of sensors increases, so does the number of interfaces to the electronics. For the practice, the sheer number of wires can become unwieldy, prone to breakage, increasing the stiffness of the system and therefore, higher resolution uniform surface systems are difficult to design and implement. One way to mitigate this issue in scalability is to use the electrodes on the top and bottom of the substrate in orthogonal rows and columns to create pixels at the intersections [1], [9]–[12], [14], [17], [20], [22]. This approach reduces the number of interfaces for an  $n$ -by- $n$  grid from  $O(n^2)$  to  $O(n)$ , a further improvement is to leverage the frequency-dependent characteristics of large-area capacitors to reduce the number of interfaces to two for an  $n \times n$  pixel array. Interrogating a capacitor at multiple frequencies effectively creates multiple sensing regions within the area of a single capacitive sensor body [23], [24], [26]. Another interesting way to reduce the number of electrodes for touch-sensing applications is to use

<sup>1</sup> Reconfigurable Robotics Lab, Institute of Mechanical Engineering, École Polytechnique Fédérale de Lausanne, Lausanne, Switzerland. <sup>2</sup>School of Engineering and Applied Science, Yale University, New Haven, CT, USA. <sup>3</sup>School of Mechanical Engineering, Purdue University, West Lafayette, IN, USA. email: jamie.paik@epfl.ch

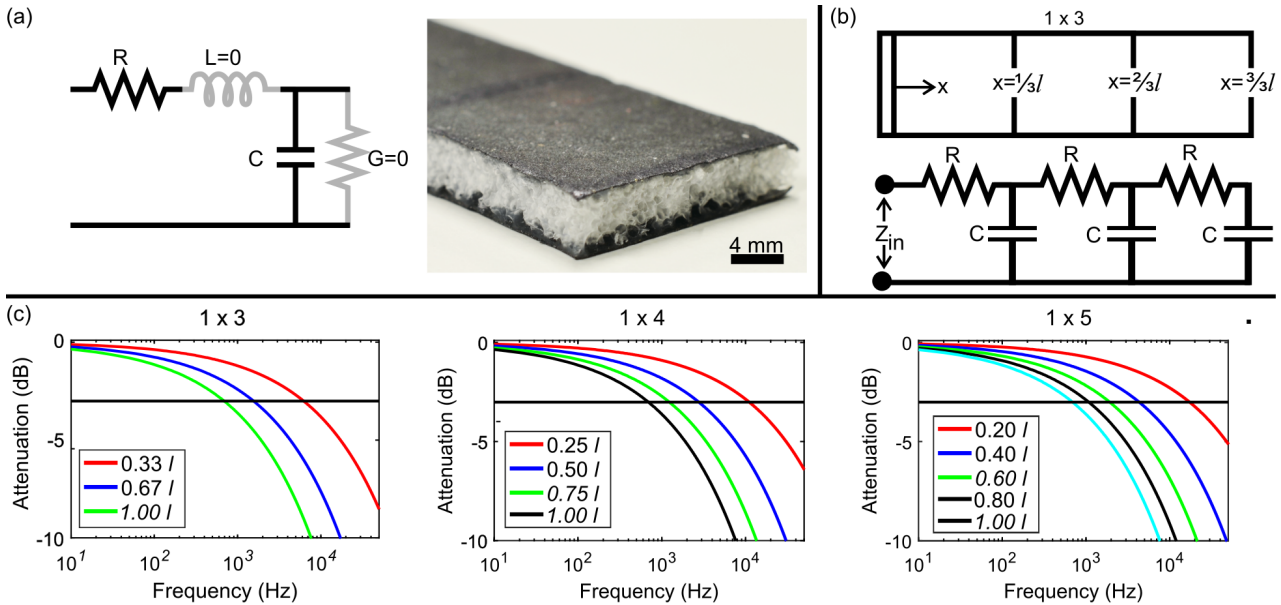


Fig. 2. Electrical equivalent circuit diagram and results of the analytical model of the 1D sensor strip. (a) Schematic of a single element in the 1D sensor strip. A photo of the sensor cross-section of the sensor strip. (b) Model of a  $1 \times 3$  pixel array. The interface is located on the left end; the distance or pixel index increases from this point along the sensor. The top schematic shows a top view of the physical device; the bottom schematic shows the corresponding electrical equivalent circuit. (c) Plots of the signal amplitude calculated at each node over a frequency sweep. The black horizontal line marks the  $-3\text{dB}$  threshold. The interrogation frequencies are the frequencies at which the signal amplitude curves intersect the  $-3\text{dB}$  line.

electric field tomography on a large conductive film [27].

In this work, we present a pressure sensing methodology for localization of point pressures on a monolithic, soft capacitive sensor (Figure 1) by interrogating the sensor at multiple frequencies to modulate the effective length of the capacitive sensor “seen” by the measurement system. Using the resistance and capacitance values of a physical sensor prototype, we developed an analytical model for the 1D representation of the capacitive sensor. Using this model, we calculated the frequency response of the sensor at different effective sensor lengths to find their corresponding cutoff frequencies. We then used the calculated cutoff frequencies as the interrogation frequencies in experimental tests. Experiments were performed by pressing at various locations on a 1D sensor strip and a 2D sensor sheet wherein the series resistance ( $R_s$ ) and parallel capacitance ( $C_p$ ) of the sensor were measured using an LCR meter at the interrogation frequencies. Because the sensors are monolithic, with no pre-determined measurement locations, we discretized the sensors into different sized pixels to attain different levels of spatial resolution. We then input the  $R_s$  and  $C_p$  values into a multi-class kernel support vector machine (KSVM) to create a classification model for localizing the point pressures. Through evaluation of the SVM using a confusion matrix, we found that we achieved between 90-100% accuracy in predicting the location of the applied pressure.

The major contributions of this work are: 1) fabrication of a monolithic soft capacitive foam skin for measuring distributed pressure locations, 2) a method to localize applied pressure by leveraging the effect of interrogating the capacitor at different frequencies, 3) demonstration of a reduction in the number of interfaces to one for a  $1 \times n$  and two for

an  $n \times n$  sensor skin while maintaining high localization accuracy.

## II. PHYSICAL EMBODIMENT

The sensors were fabricated as a large, parallel plate capacitor using a silicone and expanded graphite composite for the conductive electrodes, and silicone foam for the dielectric layer. The two components were made separately, and then glued together using a thin layer of silicone. As pressure is applied to this deformable capacitor, the thickness of the dielectric layer decreases, resulting in an increase in capacitance.

The conductive composite material was fabricated in a thin film using a rod-coating method as described in [28]. In this work, we modified the graphite loading to increase the sheet resistance from  $1 \text{ k}\Omega/\square$  to  $50 \text{ k}\Omega/\square$ , reducing the sensitivity of the sensor to electromagnetic noise and decreasing the cutoff frequency. By using a conductive composite material, it is possible to modify the sheet resistance of the capacitor’s electrodes to better accommodate the interrogation frequency capabilities of the LCR measurement system, or vice versa.

The silicone foam was fabricated by mixing silicone elastomer (DragonSkin 10 Slow, Smooth-On) with various sizes of sugar spheres (Suglets, Colorcon) to create a very soft, open-cell foam. We mixed 40 g silicone with 120 g of sugar spheres with diameters between  $500\text{-}1700 \mu\text{m}$ , and then pressed the mixture into a 4 mm deep frame to form a large, thick sheet. After the silicone cured, the sheet was submerged in  $80^\circ\text{C}$  water for 6 hours to cause the sugar to dissolve out of the foam, changing the water every hour. After allowing the water to evaporate from the pores, the foam sheet was adhered on both sides to the conductive

composite film using a thin silicone glue layer. The final area of the capacitive sensor was cut manually using a precision knife.

In addition to the customizability of the electrode sheet resistance, the unit capacitance of the sensor sheet can be modified by changing the thickness of the silicone dielectric foam. Furthermore, the stiffness of the foam can be tuned by changing the ratio of sugar spheres to silicone, or by choosing silicones of different stiffnesses.

### III. ANALYTICAL MODEL

The sensor is modeled as a network of coupled resistances and capacitances spread across the sensor plane [29]. For our application, our goal was to locate the pressure point that is effectively changing the overall sensor capacitance. The model was developed by dividing the sensor into infinitesimally small 1-dimensional resistive and capacitive components (Figure 2(a)) spread over the length of sensor (Figure 2(b)). The voltage and the current equations for modeling the sensor can then be derived from the Telegrapher's equations on an electrical transmission line [29] as follows:

$$\frac{\partial V(x, t)}{\partial x} = -(R + j\omega L)I(x, t) = -RI(x, t) \quad (1)$$

$$\frac{\partial I(x, t)}{\partial x} = -(G + j\omega C)V(x, t) = -j\omega CV(x, t) \quad (2)$$

where,  $x$  is the distance from the voltage application point and  $R$ ,  $L$ ,  $C$ , and  $G$  are the characteristic values for line components per unit length. In the case of our sensor, we have a negligible inductance ( $L \approx 0$ ) and trans-conductance ( $G \approx 0$ ) (Figure 2(a)). Combining Eq. 1 and Eq. 2, we obtain the full form of the equations as:

$$\frac{\partial^2 V(x, t)}{\partial x^2} = \gamma^2 V(x, t); \quad \frac{\partial^2 I(x, t)}{\partial x^2} = \gamma^2 I(x, t) \quad (3)$$

where, the propagation constant,  $\gamma = \alpha + j\beta = \sqrt{j\omega RC}$ .

The sensor with length  $l$  can be divided into  $n$  virtual sensor pixels, each represented as an RC couple (Figure 2(b)). In order to distinguish the pressing of each individual pixel we need at least  $n-1$  interrogation frequencies. We chose the interrogation frequencies ( $\{f_1, \dots, f_i, \dots, f_n\}$ ) to be the frequencies at which the traveling voltage wave at distances  $x_i = il/n$  for  $i \in 1 : n$  (i.e., the distance between the interface and the "end" of each pixel) is attenuated to half power.

The attenuation factor,  $\alpha$ , for the traveling voltage wave is:

$$\alpha(f) = e^{-Re(\gamma)x} = e^{(-\sqrt{\pi RC}f)x} \quad (4)$$

Hence, the attenuation functions for each pixel end point  $i$  in an  $1 \times n$  pixel sensor are:

$$\alpha_i(f) = e^{-Re(\gamma)x_i} = e^{(-\sqrt{\pi RC}f)x_i} \quad \forall i \in 1 : n \quad (5)$$

At half power attenuation,  $\alpha_i = 1/\sqrt{2}$ , and thus the interrogation frequencies can be calculated as:

$$f_i = \frac{(\ln \alpha_i(f))^2}{\pi RC x_i^2} = \frac{0.0382}{RC x_i^2} \quad \text{for } i \in 1 : n \quad (6)$$

The interrogation frequencies  $f_i$  were obtained for our 1D sensor prototype (Figure 2(a)), with dimensions  $100\text{mm} \times 20\text{mm}$ , series resistance of  $50k\Omega/\text{mm}$  and capacitance of  $108\text{fF}/\text{mm}$ . The plots of  $\alpha_i(f)$  for the  $1 \times 3$ ,  $1 \times 4$  and  $1 \times 5$  pixel sensor networks are shown in Figure 2(c). The interrogation frequencies corresponding to where  $\alpha_i = 1/\sqrt{2}$  were used in the following experimental section.

## IV. EXPERIMENTAL RESULTS

### A. Experimental Methods

We performed a series of experiments to evaluate the proposed method for localizing point pressures. Six total configurations were tested:  $1 \times n$  sensor strip and  $n \times n$  sensor skin, and by discretization the full length  $l$  into 3, 4, and 5 (virtual) pixels. In each test, we applied a  $2\text{mm}$  displacement to each pixel to double the capacitance of each pressed region. We then performed a frequency measurements at all  $f_i$  for  $1 \times n$  ( $\forall n \in 3 : 5$ ) pixel sensor array while recording the  $R_s$  and  $C_p$  values using an LCR meter (Hioki IM3253). Six repetitions of the frequency sweep for each pixel were obtained to form a feature-rich dataset. We then input these datasets ( $f_i, R_s(f_i), C_p(f_i) \forall f_i$ ) into a multi-class kernel support vector machine (KSVM) to generate a model to classify which pixel ( $1 \times n$  sensor strip) or pixel column ( $n \times n$  sensor skin reduced to  $1 \times n$  sensor strip) was pressed.

### B. K-SVM Classification

Support vectors machines are widely used in learning-based classification to divide the dataset into separate classes. While standard SVMs are designed for linear classification between binary classes using a hyper-plane passing through maximal margin of separation between the two classes [30], we require  $n$ -class classification for a  $1 \times n$  pixelated matrix. Furthermore, the non-linearity of  $R_s$  and  $C_p$  as a function of frequency (Figure 2(c)) demands a non-linear classifier model. Thus, we employed a multi-class K-SVM classification method for the pixel localization [31] using the error-correcting output codes (*ecoc*) model in the Matlab Statistics and Machine Learning Toolbox (Mathworks). For each class (pressed pixel,  $i$ ), the training data consisted of the  $R_s$  and  $C_p$  values measured in the interrogation frequency sweep.

The SVM's classification performance was assessed using a  $k$ -fold cross-validation model applied on the training data that randomly partitions the data into  $k$  sets where  $k-1$  sets was used to train the model and the remaining set was used for cross-validation of the model. The accuracy of the model was reported as a *confusion matrix*, where the model's predicted pixel (Output Class) was compared against the true pixel (Target Class).

### C. $1 \times n$ Sensor Strip

We first performed the experiments on a sensor strip that was discretized to form  $1 \times 3$ ,  $1 \times 4$ , and  $1 \times 5$  pixel arrays (Figure 3, top row). The data collected during these experiments are shown in Figure 3, middle row. As reported in the analytical model, at lower frequencies, the measured

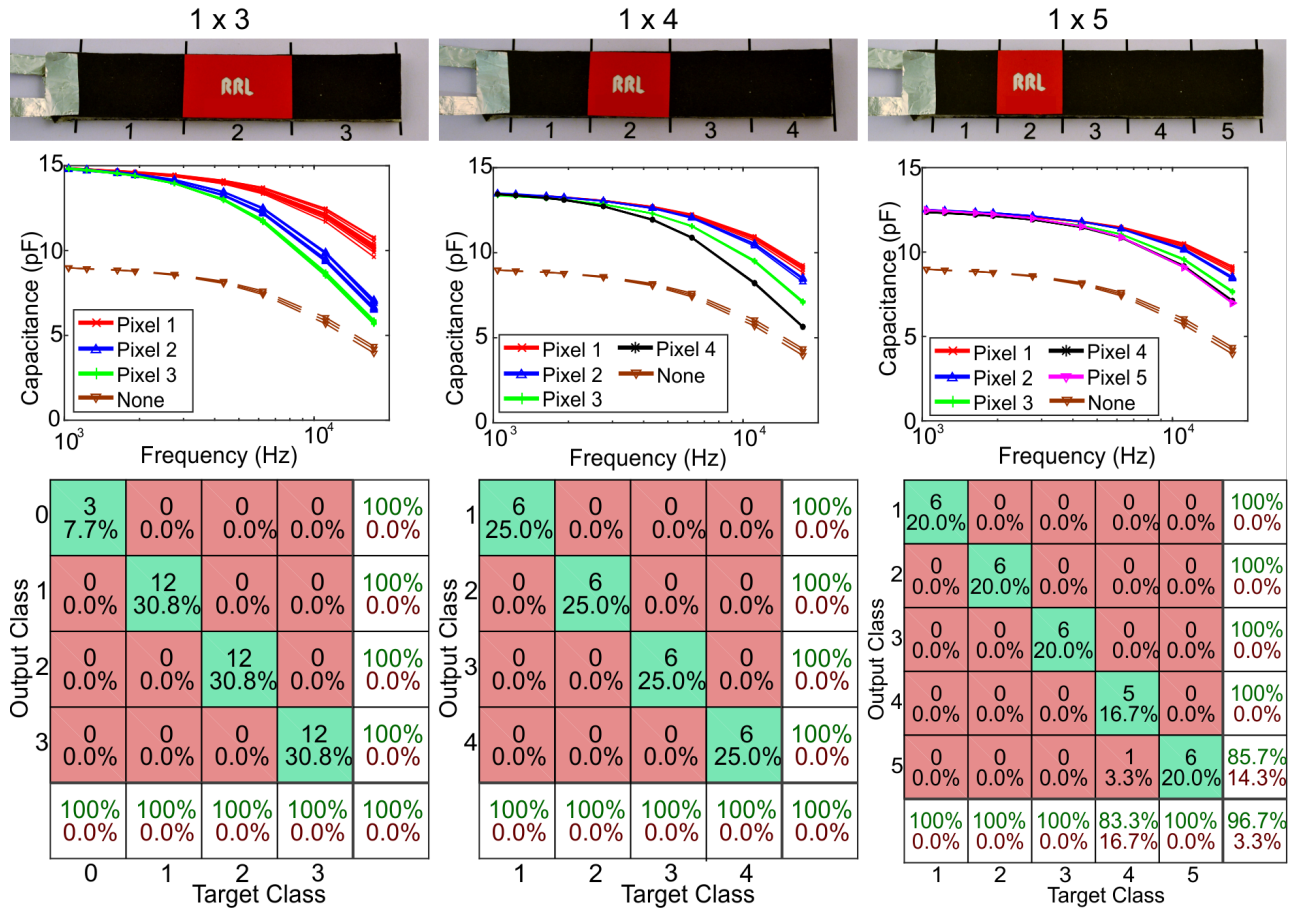


Fig. 3. Single dimensional  $1 \times n$  sensor strip experiments. (Top row) Photos of the same  $1 \times n$  sensor with differently sized pressure applicators to create 1x3, 1x4, and 1x5 pixel arrays, from left to right. (Middle row) Plots of capacitance over a frequency sweep while different pixels are pressed. (Bottom row) Confusion matrices used to evaluate the efficacy of the support vector machine in classifying each pixel press. An extra class (0) representing “No pixel pressed” in 1x3 confusion matrix shows that the model can detect when a pixel is actually pressed.

capacitance was found to be the same, regardless of which pixel is pressed. As the frequency increases however, we begin to see differentiation in the capacitance depending on which pixel was pressed. When the first pixel is pressed, a larger capacitance (relative to an un-pressed sensor) is “seen” across all interrogation frequencies. However, when a more distant pixel  $i$  is pressed, at frequencies above the cutoff frequency  $f_i$ , the effective length of the capacitor has shortened behind the pixel such that the pressed pixel is not “seen”.

The multi-class KSVM showed nearly perfect performance in classifying which pixels were pressed. The confusion matrices (Figure 3 (bottom row)) show an overall classification percentage of 100 % for the 1x3 and 1x4 tests, and 96.7 % for the 1x5 test. In the 1x5 test, the error was in misclassifying the 4th and 5th pixels. This result can be directly observed in the capacitance vs. frequency plot for the 1x5 case which shows prominent overlapping between the curves of the two most distal pixels.

#### D. $n \times n$ Sensor Skin

We expanded upon the  $1 \times n$  experiments to  $n \times n$  sensor sheets discretized into 3x3, 4x4, and 5x5 pixel arrays

(Figure 4). Our goal in this study was to correctly identify the column  $j$  in which a pixel  $(i, j)$  was pressed, when probing from the y-axis. From extension of the 1D analytical model to 2D, the cutoff frequencies were calculated to be identical to the 1D case. However, we found experimentally that the cutoff frequencies (i.e. where there were maximal differences in measured  $C_p$  and  $R_s$  depending on which column’s pixel was pressed) were in fact five times higher, ranging from 1kHz to 200kHz. We therefore interrogated the sensor at 20 frequencies logarithmically spaced between 1kHz and 200kHz to create an even more feature-rich dataset with which to build the classification model.

The results for training and prediction for  $1 \times n^{th}$  column classification are presented in Figure 4(c). It is important to note that the 2D classification results have  $n$  times lower sensitivity as 1D example. Use of 20 interrogation frequencies and feature extraction from both resistance and capacitance change of the sensor sheet improved the classification from  $\approx 60\%$  using 10 frequencies to  $>90\%$  for the 3x3 and 4x4 matrices. As the pixel size reduces, the change in capacitance from pressing a pixel relative to the overall sensor capacitance decreases. The reduction in sensitivity results

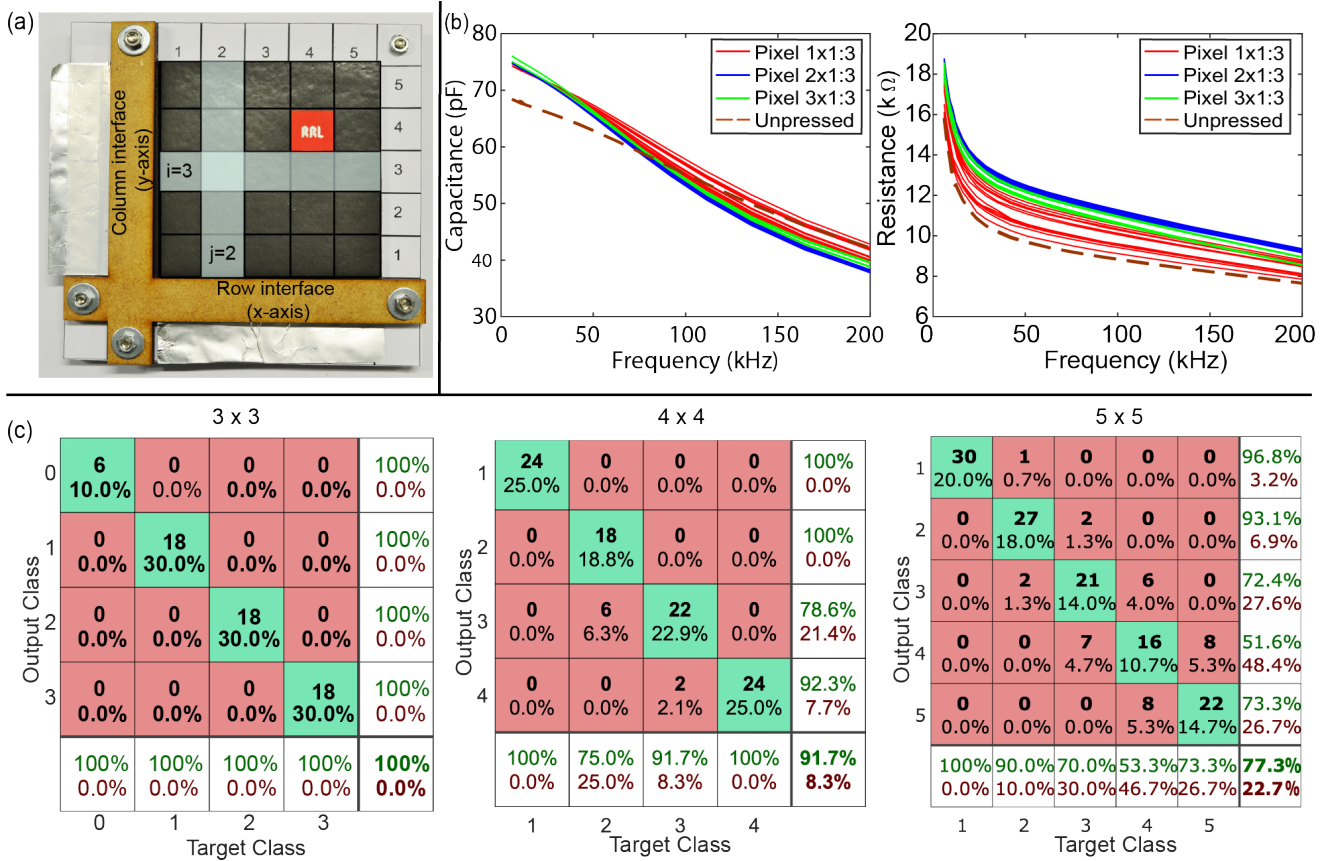


Fig. 4. (a) Photo of the 2D sensor sheet with a pressure applicator for the 5x5 pixel discretization. The foil protruding under the wood frame along the left and bottom edges was used to interface the LCR meter to the sensor electrodes. The index nomenclature is overlaid on top. (b) Frequency responses of  $R_s$  and  $C_p$  measured in the 3x3 matrix experiments. (c) Confusion matrices for the 3x3, 4x4, and 5x5 sensor configurations, respectively, after training using a multi-class support vector machine. An extra class (0) representing "No pixel pressed" was added solely to the 3x3 classification.

in a lower classification accuracy wherein the misclassified pixels are predicted to be in one of the adjacent columns (Figure 4(c) 5x5). We observe that the classification accuracy decreases at pixels furthest away from the interface, where the sensitivity of the measurement method is lowest. The performance degradation becomes even more evident as we increase the resolution beyond the 5x5 matrix, at which point the limits of the current measurement system are reached. By superimposing measurements and classifications from interrogating at both the x- and y-axes, an improved classification of pixel location can be obtained.

## V. CONCLUSION AND FUTURE WORK

We have presented a method to localize applied pressure on a soft 2D monolithic capacitive sensor. In comparison to a sensing region composed of  $n \times n$  discrete sensors, the proposed approach greatly simplifies fabrication and drastically reduces the number of interfaces from  $n^2$  to just two, facilitating integration of surface pressure measurement in soft robots. We demonstrated that pressures could be localized by interrogating the sensor at multiple frequencies to record the  $C_p$  and  $R_s$  values, and inputting those measurements into a trained kernel support vector machine to report the location of pressure in both  $1 \times n$  and  $n \times n$  pixel

arrays. We used a KSVM to perform non-linear, multi-class classification that yielded excellent results in both the  $1 \times n$  and  $n \times n$  pixel arrays.

From this preliminary study, there are many directions in which to take this work: improving localization accuracy in the 2D case, investigating the spatial resolution and load sensitivity of the system, further testing using differently shaped objects and non-flat surfaces, and measurement of multiple contact points by interrogating from more than two interface locations. To improve the localization accuracy within a 2D array, we found preliminary results that showed that the KSVM could also be used to predict the pressure location in rows (i) orthogonal to the interface (y-axis), in addition to columns (j). While the accuracy of this model expectedly is lower, the results nonetheless demonstrated that there is further information encoded in the  $R_s$  and  $C_p$  values gathered from a single interface beyond just the localization within columns parallel to the interface. Thus, we hypothesize that we can utilize the two sets of  $R_s$  and  $C_p$  values gathered by interrogating from the two axes to train four KSVMs and then convolve the KSVM models to improve localization accuracy. Furthermore, we would like to investigate the sensitivity of the system in terms of the spatial resolution. As we found in our 2D experiments, the

sensitivity of the pressure sensor reduces as we travel away from the interface. A sensitivity and information theoretic analysis [14] would provide information on the pixel size limits, based upon the magnitude of the smallest measurable capacitance change, as a function of distance from the interface.

In terms of implementation on a soft robotic system, there remain several open questions in using this system. These opportunities include measurement of continuous values of pressure, localization of multiple contact points, identification of pressure application with non-square shapes, implementation of the sensor on curved surfaces, and investigating the effect of stretch on the system. The methods that we have presented in utilizing a soft, capacitive sensor skin to localize pressure application leverages the unique properties of a large-area, deformable capacitor while providing the benefits of monolithic fabrication, more efficient interfacing, and a more physically robust device. This approach enables applications beyond soft roboticists to more easily determine interactions between soft robot systems and their surroundings, by distributing contact pressure sensing across any surface.

#### ACKNOWLEDGMENTS

This work is funded by the Swiss National Science Foundation through the National Centre of Competence in Research (NCCR) in Robotics. MCY is supported by the National Science Foundation Graduate Research Fellowship (Grant DGE-1333468).

#### REFERENCES

- [1] M. Y. Cheng, C. M. Tsao, Y. Z. Lai, and Y. J. Yang, "The development of a highly twistable tactile sensing array with stretchable helical electrodes," *Sensors and Actuators A: Physical*, vol. 166, no. 2, pp. 226–233, Apr. 2011.
- [2] J. Engel, J. Chen, and C. Liu, "Development of polyimide flexible tactile sensor skin," *J. Micromech. Microeng.*, vol. 13, no. 3, p. 359, 2003.
- [3] M. Knite, V. Teteris, A. Kiploka, and J. Kaupuzs, "Polyisoprene-carbon black nanocomposites as tensile strain and pressure sensor materials," *Sensors and Actuators A: Physical*, vol. 110, no. 1, pp. 142–149, Feb. 2004.
- [4] Y.-L. Park, C. Majidi, R. Kramer, P. Brard, and R. J. Wood, "Hyperelastic pressure sensing with a liquid-embedded elastomer," *Journal of Micromechanics and Microengineering*, vol. 20, no. 12, p. 125029, Dec. 2010.
- [5] R. K. Kramer, C. Majidi, and R. J. Wood, "Wearable tactile keypad with stretchable artificial skin," in *Robotics and Automation (ICRA), 2011 IEEE International Conference on*, 2011, pp. 1103–1107.
- [6] F. L. Hammond, Y. Meng, and R. J. Wood, "Toward a modular soft sensor-embedded glove for human hand motion and tactile pressure measurement," in *2014 IEEE/RSJ International Conference on Intelligent Robots and Systems*, Sept. 2014, pp. 4000–4007.
- [7] K. Noda, E. Iwase, K. Matsumoto, and I. Shimoyama, "Stretchable liquid tactile sensor for robot-joints," in *2010 IEEE International Conference on Robotics and Automation*, May 2010, pp. 4212–4217.
- [8] A. P. Gerratt, H. O. Michaud, and S. P. Lacour, "Elastomeric Electronic Skin for Prosthetic Tactile Sensation," *Adv. Funct. Mater.*, vol. 25, no. 15, pp. 2287–2295, Apr. 2015.
- [9] B.-Y. Lee, J. Kim, H. Kim, C. Kim, and S.-D. Lee, "Low-cost flexible pressure sensor based on dielectric elastomer film with micro-pores," *Sensors and Actuators A: Physical*, vol. 240, pp. 103–109, Apr. 2016.
- [10] H. Vandeparre, D. Watson, and S. P. Lacour, "Extremely robust and conformable capacitive pressure sensors based on flexible polyurethane foams and stretchable metallization," *Appl. Phys. Lett.*, vol. 103, no. 20, p. 204103, Nov. 2013.
- [11] S. C. B. Mannsfeld, B. C.-K. Tee, R. M. Stoltenberg, C. V. H.-H. Chen, S. Barman, B. V. O. Muir, A. N. Sokolov, C. Reese, and Z. Bao, "Highly sensitive flexible pressure sensors with microstructured rubber dielectric layers," *Nat Mater*, vol. 9, no. 10, pp. 859–864, Oct. 2010.
- [12] R. D. Ponce Wong, J. D. Posner, and V. J. Santos, "Flexible microfluidic normal force sensor skin for tactile feedback," *Sensors and Actuators A: Physical*, vol. 179, pp. 62–69, June 2012.
- [13] P. Roberts, D. Damian, W. Shan, T. Lu, and C. Majidi, "Soft-matter capacitive sensor for measuring shear and pressure deformation," in *2013 IEEE International Conference on Robotics and Automation (ICRA)*, May 2013, pp. 3529–3534.
- [14] C. Larson, J. Spjut, R. Knepper, and R. Shepherd, "OrbTouch: Recognizing Human Touch in Deformable Interfaces with Deep Neural Networks," *arXiv:1706.02542 [cs, stat]*, June 2017, arXiv: 1706.02542.
- [15] D. Kwon, T.-I. Lee, J. Shim, S. Ryu, M. S. Kim, S. Kim, T.-S. Kim, and I. Park, "Highly Sensitive, Flexible and Wearable Pressure Sensor Based on a Giant Piezocapacitive Effect of Three-Dimensional Microporous Elastomeric Dielectric Layer," *ACS Applied Materials & Interfaces*, June 2016.
- [16] J. Luo, F. R. Fan, T. Zhou, W. Tang, F. Xue, and Z. L. Wang, "Ultra-sensitive self-powered pressure sensing system," *Extreme Mechanics Letters*.
- [17] S. Yao and Y. Zhu, "Wearable multifunctional sensors using printed stretchable conductors made of silver nanowires," *Nanoscale*, vol. 6, no. 4, pp. 2345–2352, Jan. 2014.
- [18] O. Atalay, A. Atalay, J. Gafford, and C. Walsh, "A Highly Sensitive Capacitive-Based Soft Pressure Sensor Based on a Conductive Fabric and a Microporous Dielectric Layer," *Advanced Materials Technologies*, p. 1700237, Nov. 2017.
- [19] N. Farrow, L. McIntire, and N. Correll, "Functionalized textiles for interactive soft robotics," in *2017 IEEE International Conference on Robotics and Automation (ICRA)*, May 2017, pp. 5525–5531.
- [20] J. Lee, H. Kwon, J. Seo, S. Shin, J. H. Koo, C. Pang, S. Son, J. H. Kim, Y. H. Jang, D. E. Kim, and T. Lee, "Conductive Fiber-Based Ultrasensitive Textile Pressure Sensor for Wearable Electronics," *Adv. Mater.*, vol. 27, no. 15, pp. 2433–2439, Apr. 2015.
- [21] C. Larson, B. Peele, S. Li, S. Robinson, M. Tataro, L. Beccai, B. Mazzolai, and R. Shepherd, "Highly stretchable electroluminescent skin for optical signaling and tactile sensing," *Science*, vol. 351, no. 6277, pp. 1071–1074, Mar. 2016.
- [22] D. J. Lipomi, M. Vosgueritchian, B. C.-K. Tee, S. L. Hellstrom, J. A. Lee, C. H. Fox, and Z. Bao, "Skin-like pressure and strain sensors based on transparent elastic films of carbon nanotubes," *Nature Nanotechnology*, vol. 6, no. 12, p. 788, Dec. 2011.
- [23] D. Xu, A. Tairyach, and I. A. Anderson, "Stretch not flex: programmable rubber keyboard," *Smart Mater. Struct.*, vol. 25, no. 1, p. 015012, 2016.
- [24] D. Xu, A. Tairyach, and I. Anderson, "Where the rubber meets the hand: Unlocking the sensing potential of dielectric elastomers," *J. Polym. Sci. Part B: Polym. Phys.*, no. 4, pp. 465–472, Feb. 2016.
- [25] M. Acer, M. Salerno, K. Agbeviade, and J. Paik, "Development and characterization of silicone embedded distributed piezoelectric sensors for contact detection," *Smart Materials and Structures*, vol. 24, no. 7, p. 075030, 2015.
- [26] E. L. White, M. C. Yuen, and R. K. Kramer, "Distributed sensing in capacitive conductive composites," in *Proceedings of IEEE Sensors*, 2017.
- [27] Y. Zhang, G. Laput, and C. Harrison, "Electrick: Low-Cost Touch Sensing Using Electric Field Tomography." ACM Press, 2017, pp. 1–14.
- [28] E. L. White, M. C. Yuen, J. C. Case, and R. K. Kramer, "Low-Cost, Facile, and Scalable Manufacturing of Capacitive Sensors for Soft Systems," *Adv. Mater. Technol.*, vol. 2, no. 9, pp. n/a–n/a, Sept. 2017.
- [29] H. Meng, S. Chen, Y. L. Guan, C. L. Law, P. L. So, E. Gunawan, and T. T. Lie, "A transmission line model for high-frequency power line communication channel," in *Proceedings. International Conference on Power System Technology*, vol. 2, 2002, pp. 1290–1295 vol.2.
- [30] M. A. Hearst, S. T. Dumais, E. Osuna, J. Platt, and B. Scholkopf, "Support vector machines," *IEEE Intelligent Systems and their Applications*, vol. 13, no. 4, pp. 18–28, July 1998.
- [31] J. Weston and C. Watkins, "Multi-class support vector machines," Technical Report CSD-TR-98-04, Department of Computer Science, Royal Holloway, University of London, May, Tech. Rep., 1998.